Iranian Journal of Astronomy and Astrophysics
Vol. 11, No. 4, Autumn 2024, 311–324
©Available online at http://ijaa.du.ac.ir
DOI: 10.22128/ijaa.2025.932.1204
Online ISSN: 2383–403X

Iranian Journal of Astronomy and Astrophysics

Research Paper

Magnetic Braking of the Rotational Molecular Cloud Cores, Revisited

Abbas Ebrahimi*[1] · Mohsen Nejad-Asghar[2]

[1] Department of Theoretical Physics, Faculty of Science, University of Mazandaran, P. O. Box 47416-95447, Babolsar, Iran;
*E-mail: abbas_ebri@stu.umz.ac.ir

[2] Department of Theoretical Physics, Faculty of Science, University of Mazandaran, P. O. Box 47416-95447, Babolsar, Iran;
E-mail: nejadasghar@umz.ac.ir

Received: 28 December 2024; **Accepted:** 9 May 2025; **Published:** 17 May 2025

Abstract. The phenomenon of magnetic braking is one of the significant physical effects of the magnetic field in rotating molecular clouds. Here, we revisit the work of Nakano (1989). In addition to receiving his results, we investigate the effects of the density ratio (between periphery of the core to its mean density), and the density condensations around the core. We consider the density profile of the surrounding medium as $r^{-\eta}$, where r is the distance from the core center and η is a constant between 0 and 4. Regarding the presence of some dense regions around the molecular cloud cores, a Gaussian function is added to the density profile to represent these condensations in the surrounding medium. The numerical method is used in the Laplace space to ascertain the dependency of the angular velocity of the core to the time. The results show that for larger η values, the time scale of the magnetic braking increases. Moreover, the presence of condensation does not have a significant effect on the magnetic braking. Also, the the results show that the magnetic braking being stronger with increasing density ratio. This increasing indicates that the magnetic field is more firmly bonded to the bulk materials. This effect strengthens the magnetic tension force and slows down the core faster that indicates the importance of the magnetic braking. The results show that increasing density slope and/or decreasing density ratio are somewhat effective in weakening the magnetic braking and resolving its catastrophic effect.

Keywords: Stars: formation, ISM: magnetic fields, Methods: numerical, ISM: clouds, MHD

1 Introduction

One of the interesting phenomena in the interstellar medium is the formation of stars and planets. Various physical mechanisms, such as magnetic field, turbulent, rotation, etc., are influential in the process of star formation and its by-products (i.e., planets). The rotation-incorporated magnetic fields have several important physical effects on the molecular clouds(e.g. [1]). One of these significant physical effects is the magnetic braking [2], which arises from the stress caused by the bending of magnetic field lines. This mechanism

* *Corresponding author*

was first investigated by [3] to study the transport of angular momentum, from a massive cold gas cloud through the hot galactic background, by the propagation of Alfvén waves. The time-scale of the magnetic braking on the evolution of molecular cloud disks and cores was investigated by some pioneer authors (e.g. [4–6]).

The magnetic braking process is also efficient in the collapse and fragmentation of molecular clouds, which was first investigated by [7] for a rotating toroidal magnetized core, and by [10] and [11] for the collapse and fragmentation of the prolate and oblate molecular clouds. Studies showed that by assuming an ideal MHD and with the magnetic field aligned with the rotational axis of the core, the magnetic braking disrupts the formation of disks around the protostars (e.g. [16,27]). The disk formation depends on two main parameters which control the efficiency of magnetic braking: the ratio of azimuthal and vertical components of the magnetic field at the disk surface, and the Alfvén speed in the surrounding medium. The high efficiency of the magnetic braking and disruption of disk formation around the protostars is known as the magnetic braking catastrophe [17].

Three suggestions are presented to resolve the magnetic braking catastrophe: (1) non-ideal MHD effects including ambipolar diffusion (e.g. [14,24,28,42,44,46,47]), Ohmic dissipation (e.g. [13,14,37,41,42]), and the Hall effect (e.g. [23,26,38,48]), (2) misalignment between rotational axis and magnetic field (e.g. [12,18,20,22,23,45]), and (3) turbulence and the dynamical nature of the environment (e.g. [25,33–35,43]).

The net effect of magnetic braking on a dense core is due to the actual degree of the magnetic fields twisting, and the propagation of the torsional Alfvén waves into the surrounding medium. Thus, the properties of the surrounding medium can influence the magnetic braking efficiency. For example, [30] (hereafter N89) analytically analyzed the effect of variations of the ambient density, around a rotating core, on the magnetic braking time scale. He considered the variation of density in the surrounding medium as $r^{-\eta}$, where r is the distance from the core center and η is a constant between 0 and 4. For $\eta = 4$, the results show an exponential decline in the core angular velocity with respect to time t. For $0 \leq \eta < 4$, the core angular velocity has two decreasing (over time) components: one component decreases exponentially with t and the other decreases proportional to $t^{-(10-2\eta)/(6-\eta)}$ at large t values. The surrounding medium of the molecular cloud cores also have complex structure with fragmentation and small condensations (e.g. [15,19,21]). These density condensations in the ambient medium may also influence the magnetic braking efficiency.

Here, we revisit the work of N89, who used an analytical method to solve the equations and determine the magnetic braking time scales. In the case of $\eta = 4$, an exact analytical solution was obtained, while for $0 \leq \eta < 4$, N89 used the approximation of $\rho(Z) \ll \rho_{cc}$, where $\rho(Z)$ is the density at the periphery of core (where a layer approximation for the core can be used) and ρ_{cc} is the core mean density. Numerical methods must be used to solve the equations without considering the above approximation and determine the time scale of the magnetic braking for the $0 \leq \eta < 4$ case. In this way, not only the solutions of N89 are obtained, but we can also extend the work to consider the effects of the density ratio, $\rho(Z)/\rho_{cc}$, and also density condensations. For this purpose, in § 2, we formulate the problem as outlined by N89. In § 3, by transforming to the Laplace space, the same equations are derived for the core angular velocity. In the following, we express the method of numerical solution. In § 4, the results are given. The effect of density condensations on the magnetic braking is considered in § 5. Finally, § 6 is devoted to a summary and conclusions.

2 Formulation of the problem

We consider a rigidly rotating core inside an axisymmetric molecular clump in spherical polar coordinates (r, θ, ϕ). We neglect the contraction/expansion of the clump ($v_r \approx 0$) with negligible poloidal velocity ($v_\theta \approx 0$) so that we have a purely rotatory motion with $v_\phi = \varpi\Omega$, where Ω is the angular velocity and $\varpi = r\sin\theta$ is the distance from the symmetry axis.

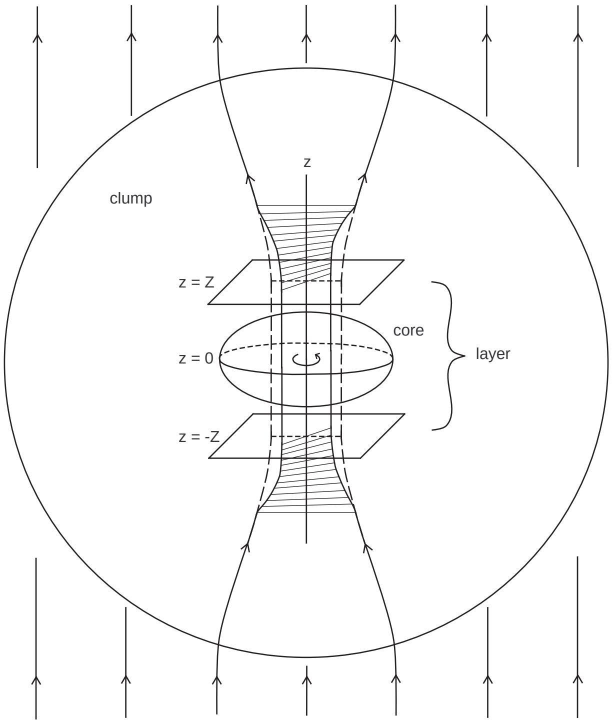

Figure 1: Schematic diagram of the magnetic configuration around an oblate core and its surrounding clump. The magnetic field is assumed to be uniformed outside the clump. The layer is assumed to rotate rigidly whit the core, so that the torsional Alfvén waves (twisted field lines depicted as shaded regions) propagate outside this layer. The toroidal components of the twisted magnetic field lines create a braking torque that counteract the spinup of the core/layer and lowers its angular velocity.

We adopt the magnetic configuration as outlined by a schematic diagram in the Figure 1. We assume that the magnetic fields are well frozen into the core and its ambient clump. The rotation of the cloud core through the ambient medium, bends the magnetic fields so that a torsional Alfvén wave will propagate through the clump (e.g., [36]). The Alfvén velocity,

$$v_A = 1.5 \left(\frac{B}{10\mu\mathrm{G}}\right) \left(\frac{n}{10^2\mathrm{cm}^{-3}}\right)^{-\frac{1}{2}} \mathrm{km\,s}^{-1}, \tag{1}$$

is much greater than the rotational velocity in a typical clump region,

$$v_\phi = 0.03 \left(\frac{\Omega}{10^{-14}\mathrm{s}^{-1}}\right) \left(\frac{\varpi}{0.1\mathrm{pc}}\right) \mathrm{km\,s}^{-1}, \tag{2}$$

so that we focus our attention around the symmetry axis in which $B_\theta \approx 0$ and $B_r \propto r^{-2}$. The magnetic induction equation for a purely rotatory motion with $\mathbf{v} = \mathbf{e}_\phi v_\phi$, leads to $\partial B_r/\partial t = \partial B_\theta/\partial t = 0$. Thus, B_r is independent of the time, and $B_\theta = 0$ at all the times.

Assuming that both the fluid configuration and the field are axisymmetric, the only functional component of the magnetic torque on the element is along the symmetry axis (with unit vector $\mathbf{e}_z$). This component exerted on the gas around the symmetry axis of the clump, as measured per unit volume, is

$$\gamma_z \mathbf{e}_z = \varpi \mathbf{e}_\varpi \times \frac{1}{4\pi}[(\nabla \times \mathbf{B}) \times \mathbf{B}]_\phi. \tag{3}$$

On the other hand, this torque is equal to the rate of change of the gas angular momentum, $\gamma_z = \partial(\rho \varpi v_\phi)/\partial t$, where ρ is the density of the clump. In this way, equation (3) can be rewritten as

$$\frac{\partial v_\phi}{\partial t} = \frac{B_r}{4\pi\rho}\frac{1}{r}\frac{\partial}{\partial r}\left(r B_\phi\right), \tag{4}$$

Differentiating this equation with respect to t, and using the ϕ-component of the magnetic induction equation,

$$\frac{\partial B_\phi}{\partial t} = \frac{1}{r}\frac{\partial}{\partial r}\left(r v_\phi B_r\right), \tag{5}$$

with the relation $v_\phi = \Omega r \sin\theta$, we have

$$\frac{\partial^2 \Omega}{\partial t^2} = \frac{[B_r(Z)]^2}{4\pi (r/Z)^2 \rho}\frac{\partial^2 \Omega}{\partial r^2}, \tag{6}$$

where $B_r = B_r(Z)(r/Z)^{-2}$ is used, where $B_r(Z)$ is the magnetic field at the point $z = Z$, above the core's pole.

We consider two points on the symmetry axis, with a short distance from the poles, outside the core. The coordinates of these points are $z = -Z$ and $z = Z$ relative to the core center. We assume that the layer between these points rotates rigidly with the core, and solve the propagation of the torsional Alfvén wave outside this layer. The continuity of the field lines, between the layer surfaces and the clump gas, requires that the angular velocity of the layer be equal to $\Omega(r = Z, t)$. The angular velocity of the layer changes with time according to $I d\Omega(r = Z, t)/dt = N$, where

$$N = 2\varpi B_z(\varpi, Z, t) B_\phi(\varpi, Z, t)/4\pi, \tag{7}$$

is the torque exerted on the layer per unit area (by assuming symmetry with respect to midplane $z = 0$), and $I = \sigma\varpi^2$ is the moment of inertia per unit area, where σ is the column density of layer along the z-axis. Substituting I and N into the equation of rotational motion of the layer, and differentiating with respect to t, leads to

$$\frac{d^2\Omega(r = Z, t)}{dt^2} = \frac{[B_r(Z)]^2}{2\pi\sigma}\left(\frac{\partial \Omega}{\partial r}\right)_{r=Z}, \tag{8}$$

where the ϕ-component of the magnetic induction equation (5) is also used.

The density distribution of the clump at $r \geq Z$ is assumed as

$$\rho(r) = \rho(Z)\left(\frac{r}{Z}\right)^{-\eta}, \tag{9}$$

where $\rho(Z)$ is the density at the periphery of core (where a layer approximation for the core can be used) and η is a constant between 0 and 4.

We use the scale values of length and time equal to Z and $Z/v_A(Z)$, respectively, where $v_A(Z) \equiv B_r(Z)/[4\pi\rho(Z)]^{1/2}$ is the Alfvén velocity at $r = Z$. In this way, we rewrite the equations (6) and (8) as

$$\frac{\partial^2\Omega}{\partial\tau^2} = \frac{1}{\xi^{4-\eta}}\frac{\partial^2\Omega}{\partial\xi^2}, \quad \xi > 1, \tag{10}$$

$$\frac{d^2\Omega(\xi=1,t)}{d\tau^2} = \frac{\rho(Z)}{\rho_L}\left(\frac{\partial\Omega}{\partial\xi}\right)_{\xi=1}, \tag{11}$$

where $\xi \equiv r/Z$ is the non-dimensional length, $\tau \equiv tv_A(Z)/Z$ is the non-dimensional time, and $\rho_L \equiv \sigma/2Z$ is the layer (and also the core) mean density.

3 Solution method

The Laplace transform of the equation (10), with initial condition $\Omega = \partial\Omega/\partial\tau = 0$, at $\tau = 0$ for clump gas ($\xi > 1$), is

$$s^2\tilde{\Omega} = \frac{1}{\xi^{4-\eta}}\frac{\partial^2\tilde{\Omega}}{\partial\xi^2}, \tag{12}$$

where

$$\tilde{\Omega}(\xi,s) = \int_0^\infty \Omega(\xi,\tau)e^{(-s\tau)}d\tau, \tag{13}$$

is the Laplace transform of $\Omega(\xi,\tau)$. Equation (12) can be reduced to the modified Bessel equation, with physical solution as

$$\tilde{\Omega}(\xi,s) = A(s)\xi^{1/2}K_\nu(2s\nu\xi^{1/2\nu}), \tag{14}$$

where $\nu \equiv 1/(6-\eta)$, and $A(s)$ depends on the boundary conditions. Substituting equation (14) into the Laplace transform of equation (11),

$$s^2\tilde{\Omega}(\xi=1,s) - s\Omega_0 = \frac{\rho(Z)}{\rho_L}\left(\frac{\partial\tilde{\Omega}}{\partial\xi}\right)_{\xi=1}, \tag{15}$$

where $\Omega_0 = \Omega(\xi=1,\tau=0)$ is the initial angular velocity of the core (and also the layer) with initial condition $d\Omega(\xi=1,\tau)/d\tau = 0$ at $\tau = 0$, we obtain

$$A(s) = \Omega_0\left[sK_\nu(2s\nu) + \frac{\rho(Z)}{\rho_L}K_{\nu-1}(2s\nu)\right]^{-1}. \tag{16}$$

By substituting the relation (16) into the result (14), and then using the inverse Laplace transform, we obtain

$$\Omega(\xi=1,\tau) = \frac{\Omega_0}{2\pi i}\int_{\gamma-i\infty}^{\gamma+i\infty}\frac{K_\nu(2s\nu)e^{s\tau}}{sK_\nu(2s\nu) + [\rho(Z)/\rho_L]K_{\nu-1}(2s\nu)}ds, \tag{17}$$

for the angular velocity of the core. The integrand in this equation is a multi-valued function on the complex s-plane and the exact analytical evaluation of the integral is rather difficult. N89 evaluated this integral approximately by assuming that the surface layer density, $\rho(Z)$, is much smaller than its mean density, ρ_L. He found that the angular velocity of the core oscillates with an amplitude decreasing exponentially.

Here, we use an approximately numerical method to evaluate the solution of equation (17). We know that the magnetic braking (or damping) is a consequence of the Eddy currents across the magnetic field lines. These currents, which are theoretically derived from the Lenz's law (represented in equation 5), are also investigated by many experiments (e.g., [9,29]). For example, the experiment of a magnetic pendulum bob above a metal plate show that the Eddy currents created in the metal plate cause the magnetic braking to decay the pendulum angular position as a damped oscillatory motion (e.g., [31,40]). According to this physical view of the magnetic braking effect, we are looking for the damped oscillatory solution to solve the equation (17). Of course, we must note that slowing down the rotation of the core due to the magnetic braking is not a continuous pendulum-like motion, i.e., its decreasing functionality has a physical meaning only before the first zero of the angular velocity. For this purpose, we choose an oscillating function with exponentially decreasing amplitude as

$$\Omega(\xi = 1, \tau) = \gamma e^{-\alpha c\tau} \cos(kc\tau) - (\gamma - \Omega_0)e^{-\beta c\tau}, \tag{18}$$

where the initial condition $\Omega(\xi = 1, \tau = 0) = \Omega_0$ is satisfied, and γ, α, c, k and β are constants. The Laplace transform of the equation (18) is (e.g., [8])

$$\tilde{\Omega}(\xi = 1, s) = \frac{\gamma}{c} \frac{\frac{s}{c} + \alpha}{\left(\frac{s}{c} + \alpha\right)^2 + k^2} - \frac{(\gamma - \Omega_0)}{c} \frac{1}{\left(\frac{s}{c} + \beta\right)}. \tag{19}$$

The condition $\lim_{s\to\infty} \tilde{\Omega} = 0$ is satisfied, and the condition $\lim_{s\to 0} \tilde{\Omega} = 0$ leads to

$$\gamma = \Omega_0 \frac{\frac{1}{\beta}}{\frac{1}{\beta} - \frac{\alpha}{\alpha^2+k^2}}. \tag{20}$$

Thus, here, we have four unknown parameters α, β, c and k.

The basic approach in our numerical method is to adjust the best fitted values of the four parameters $a_1 \equiv \alpha$, $a_2 \equiv \beta$, $a_3 \equiv k$, and $a_4 \equiv c$, so that the merit function (19) yields to the best-fit-result of the integrand of equation (17). For this purpose, we define a chi-square nonlinear merit function and determine the best-fit parameters by its minimization using some iterative methods. Here, we use the Levenberg-Marquardt method as outlined by Press et al. (1992).

4 Results

To investigate the effect of the magnetic braking of the core, we transformed the equations (10) and (11) into the Laplace space and achieved the integral (17). The exact analytical evaluation of the integral (17) is rather difficult. The integration for the case of $\nu = 1/2$ can be performed analytically. The solution in this case is investigated by N89 as

$$\Omega(\xi = 1, \tau) = \Omega_0 \exp\left(-\frac{\rho(Z)}{\rho_L}\tau\right). \tag{21}$$

He also evaluated the equation (17) by assuming the approximation $\rho(Z) \ll \rho_L$. The approximate results show that the behavior of the angular velocity, $\Omega(\xi = 1, \tau)$, is oscillatory decay (e.g., [3,4,30]). Here, we applied a damping oscillatory function (18) whose Laplace transform, according to the Laplace transform tables, is represented by the equation (19). In this way, there is no need to solve the integral in equation (17) analytically because the equation (19) is the inverse Laplace of the chosen equation (18).

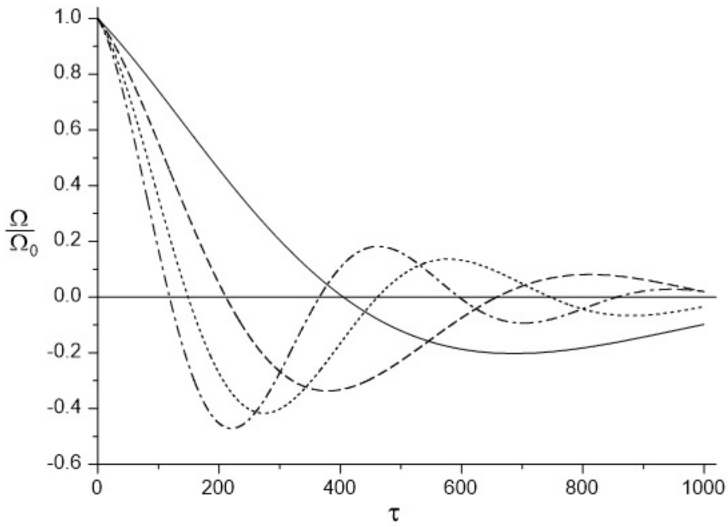

Figure 2: Angular velocity of the core vs. non-dimensional time, for $\rho(Z)/\rho_L = 10^{-3}$ and $\nu = 1/3$ (solid), $\nu = 1/4$ (dash), $\nu = 1/5$ (dot), and $\nu = 1/6$ (dash-dot).

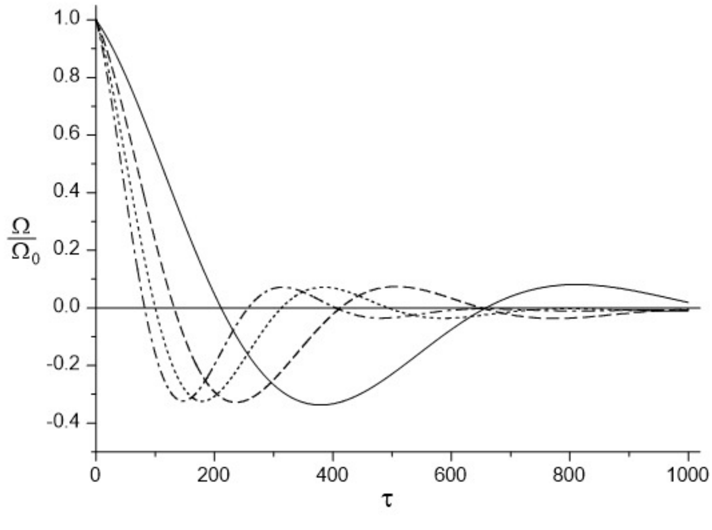

Figure 3: Angular velocity of the core vs. non-dimensional time, for $\nu = 1/4$ and $\rho(Z)/\rho_L = 1 \times 10^{-3}$ (solid), $\rho(Z)/\rho_L = 2 \times 10^{-3}$ (dash), $\rho(Z)/\rho_L = 3 \times 10^{-3}$ (dot), and $\rho(Z)/\rho_L = 4 \times 10^{-3}$ (dash-dot).

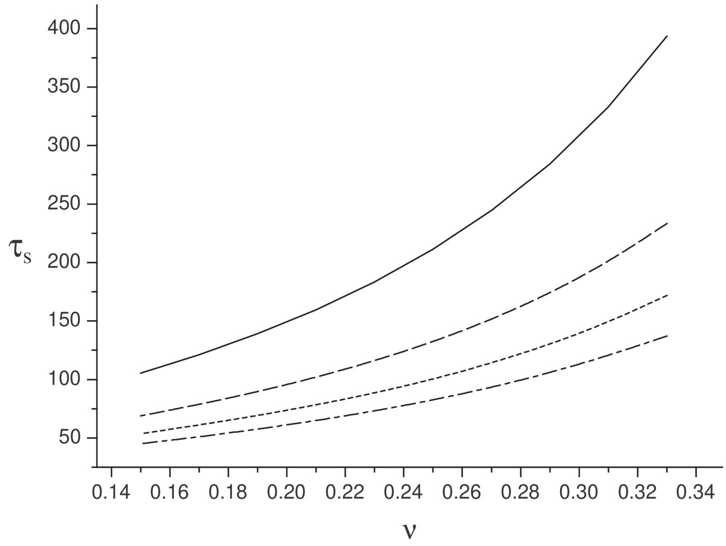

Figure 4: Non-dimensional stop-time according to the varies values of ν, for $\rho(Z)/\rho_L = 1 \times 10^{-3}$ (solid), $\rho(Z)/\rho_L = 2\times10^{-3}$ (dash), $\rho(Z)/\rho_L = 3\times10^{-3}$ (dot), and $\rho(Z)/\rho_L = 4\times10^{-3}$ (dash-dot).

Here, in addition to the effect of ν, we want to examine the effects of the density ratio, $\rho(Z)/\rho_L$, on the behavior of the core angular velocity and the magnetic braking. For this purpose, we use the numerical method. Equation (19) has four parameters: α, c, k and β. We can determine these four parameters by fitting the equation (19) to the integrand of the equation (17). To investigate the effect of ν, we choose $\rho(Z)/\rho_L = 10^{-3}$. For $\nu = 1/3$, 1/4, 1/5 and 1/6, we find the best parameters. Figure 2 shows the angular velocity function (18) versus the non-dimensional time. Then, we choose a typical value of $\nu = 1/4$, and examine the effect of the various values of the density ratio $\rho(Z)/\rho_L$. Here, we choose $\rho(Z)/\rho_L = 1 \times 10^{-3}$, 2×10^{-3}, 3×10^{-3}, and 4×10^{-3}, and find the best fitted parameters. The angular velocity function (18) versus the non-dimensional time is shown in Figure 3.

The figures 2 and 3 show the damping oscillating functions, which are due to the magnetic braking effects on the rotational core. These curves, which include multiple zeros, are just the mathematical results of solving the equation (17). It is obvious that due to the dynamical behavior of gases, the angular velocity of the molecular cloud cores never reaches to zero. Physically, only the decreasing behavior of the angular velocity before the first zero is desired. There is not any physical reasoning behind the obtained first zero in the solution. Here, we defined a stop-time, τ_s, which indicates the point where the core angular velocity, $\Omega(\xi = 1, \tau)$, reaches to the first zero. In dimensional time we have

$$t_s = 6.3 \times 10^4 \, \tau_s \left(\frac{v_A}{1.5\mathrm{km\,s^{-1}}}\right)^{-1} \left(\frac{Z}{0.1\mathrm{pc}}\right) \text{ yr.} \tag{22}$$

The change of τ_s with respect to ν, for different density ratios, is shown in Figure 4. Also, the changes of τ_s in terms of $\rho(Z)/\rho_L$, for different values of ν, are plotted in Figure 5.

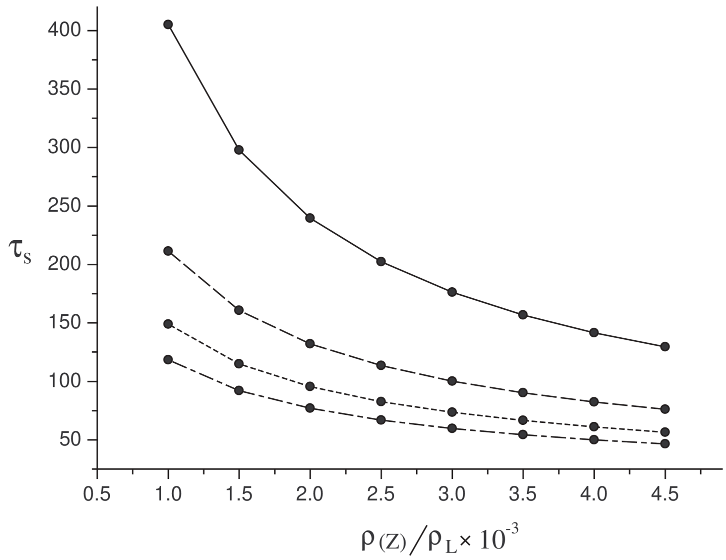

Figure 5: Non-dimensional stop-time according to the varies values of $\rho(Z)/\rho_L$, for $\nu = 1/3$ (solid), $\nu = 1/4$ (dash), $\nu = 1/5$ (dot), and $\nu = 1/6$ (dash-dot).

5 The effect of density condensation

In this section, instead of density distribution (9), we use

$$\rho(r) = \rho(Z) f(r) \left(\frac{r}{Z}\right)^{-\eta}, \tag{23}$$

where

$$f(r) = 1 + \varepsilon e^{-\left(\frac{r-r_c}{\Delta}\right)^2}, \tag{24}$$

is a Gaussian function representing the condensation in the surrounding medium, with the amplitude ε and width $\approx 2\Delta$, at distance $r_c > Z + \Delta$ from the core center. Using this density profile in the equations (6) and (8), after Laplace transformation, we have

$$s^2 \tilde{\Omega} = \frac{1}{\xi^{4-\eta} f(\xi)} \frac{\partial^2 \tilde{\Omega}}{\partial \xi^2}, \tag{25}$$

instead of the equation (12).

With physical solution as $\tilde{\Omega}(\xi, s) = A(s)\xi^{1/2} Y_\nu(x)$, instead of the known modified Bessel equation (14), here, equation (25) leads to

$$x^2 Y_\nu^{''}(x) + x Y_\nu^{'}(x) - \left[x^2 f_\nu(x) + \nu^2\right] Y_\nu(x) = 0, \tag{26}$$

where $x \equiv 2s\nu\xi^{1/2\nu}$ and

$$f_\nu(x) = 1 + \varepsilon e^{-\left(\frac{x^{2\nu} - x_c^{2\nu}}{\delta^{2\nu}}\right)^2}, \tag{27}$$

where $x_c \equiv 2s\nu\xi_c^{1/2\nu}$ and $\delta \equiv 2s\nu(\Delta/Z)^{1/2\nu}$. If $\varepsilon \to 0$, then, the differential equation (26) becomes the modified Bessel differential equation whose answer is known as $K_\nu(x)$. Here, we assumed that the function $Y_\nu(x)$ is equal to the modified Bessel function in the regions of

$x \gg x_c$ and $x \ll x_c$ as the boundaries of the differential equation (26). In this way, the two point boundary value problem of the differential equation (26) can be numerically solved using the *shooting* or *relaxation* methods [32].

Similar to derivation of the equation (17), we reach to

$$\Omega(\xi = 1, \tau) = \frac{\Omega_0}{2\pi i} \int_{\gamma - i\infty}^{\gamma + i\infty} \frac{Y_\nu(2s\nu) e^{s\tau}}{sY_\nu(2s\nu) - [\rho(Z)/\rho_L]\left[\frac{1}{2s} Y_\nu(2s\nu) + Y'_\nu(2s\nu)\right]} ds, \tag{28}$$

for the angular velocity of the core. Here, we use the proposed numerical method to solve the equation (17) to find the best fitted parameters for the angular velocity concerned to the opted density profile (23). For this porpous, we fit the merit function (19) to the integrand of the equation (28) to obtain the four parameters α, β, k, and c.

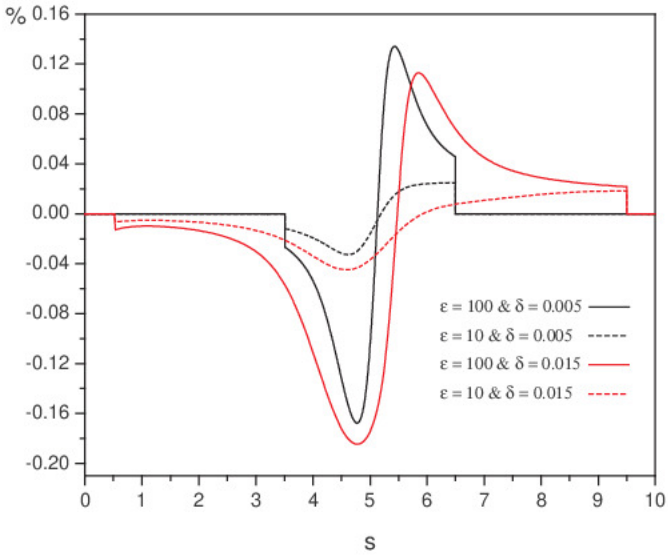

Figure 6: Percentage difference between the integrands of the equations (28) and (17), $\frac{\tilde{\Omega}_Y - \tilde{\Omega}_B}{\tilde{\Omega}_B} \times 100$, where $\tilde{\Omega}_Y$ and $\tilde{\Omega}_B$ are their integrands, respectively. Here, we choose $\nu = 1/4$, $\rho(Z)/\rho_L = 10^{-3}$ and $x_c = 2.5$.

The equation (27) is a Gaussian function representing the condensation in the surrounding medium with two important parameters: ε and δ. Here, we choose $x_c = 2.5$ and solve the equation (28) with $\varepsilon \leq 100$ and $\delta \leq 0.015$. Figure 6 shows the percentage difference between the integrands of the equations (28) and (17), versus s. As can be seen from the Figure 6, this percentage difference is less than 0.16%. Thus, our method to solve the equation (28) shows that the presence of condensations in the surrounding medium does not have a significant effect on the magnetic braking of the core.

6 Summary and conclusions

The purpose of this research is to re-examine the magnetic braking of a rotating molecular cloud core which was previously approximated in an analytical method by N89. He assumed that the density ratio of the surrounding medium (core periphery) to the core mean density was much smaller than unity. In this way, he succeeded to analytically solve the problem by using some approximations. To investigate the effects of the density ratio and the existence of the condensations in the surrounding medium, we formulated the problem as outlined by N89, and solved numerically.

Figure 1 schematically depicts the configuration of the magnetic fields for a rotating core inside a clump, and the propagation of the Alfvén waves that cause magnetic braking. By transforming to the Laplace space, the angular velocity of the core can be obtained by solving the Laplace inverse transformation integral (17). The inverse Laplace transform can be determined in various ways such as the calculus of residues, numerical approach, and a table of transforms (e.g., [8]). Here, we used the table transform to present the solution of the equation (17) by a damped oscillating function (18), whose Laplace transform is given by function (19). By fitting the function (19) on the integrand of the equation (17), the four parameters: α, β, c, and k can be obtained which can be used to plot the function (18) for different values of ν and $\rho(Z)/\rho_L$.

The case of $\nu = 1/2$, whose exact analytical answer is expressed by the equation (21) is solved by the above numerical approach. The parameters were as follows $\alpha = \rho(Z)/\rho_L$, $\beta = 0$, $c = 1$, and $k = 0$. The effect of different values of ν on the angular velocity of the core for a typical density ratio is shown in Figure 2. For smaller ν values, the angular velocity of the core decreased over a shorter period of time, therefore, the magnetic braking acts more strongly. According to $\nu = 1/(6 - \eta)$ and the density distribution (9), the values of ν change the form of radial density dependence of Alfvén waves propagation environment in the clump. The steep density distribution, $\propto 1/r^4$, corresponds to $\nu = 1/2$. In this case, the effect of the magnetic braking on the angular velocity of the core has an exact solution in the form of an exponential function (21). For $\eta = 0$, the density of clump is constant, thus, the minimum ν will be equal to 1/6. By reducing ν from 1/2 to 1/6, the slope of the density function decreases. Based on the Figure 2, the magnetic braking becomes stronger as the density slope by decreasing r. Physically, the propagation of the Alfvén waves through the clump medium transport the angular momentum of the core, thereby, reducing its angular velocity. The rotating core significantly slows down when the Alfvén waves set into rotational motion and the amount of clump matter with the moment of inertia equals to that of the core. For lower density slope of the clump medium, a shorter time is required for the moment of inertia of the ambient material to be equal to the moment of inertia of the core. Therefore, the reduction of ν strengthens the magnetic braking as shown in Figure 2.

To investigate the effect of density ratios, we considered typically $\nu = 1/4$. The angular velocity of the core is plotted versus the non-dimensional time in Figure 3 for $\rho(Z)/\rho_L = 1, 2, 3$, and 4×10^{-3}. As seen, the effect of magnetic braking increases in the larger density ratios. For the case where the density drops more slowly from the core center to the surface of the layer, the density ratio $\rho(Z)/\rho_L$ will be higher. Increasing of the density ratio implies an increase in charged particles close to the surface of the layer. According to the flux freezing assumption, the increase in the charged particles increases the dependence of the magnetic field lines on the bulk materials in this region. Such an increase in the dependence of the magnetic field to the bulk materials strengthens the magnetic tension force and thus, slows down the layer faster and increases the importance of magnetic braking.

A dimensional time scale is presented in the equation (22) which quantifies the time needed for the core (as well as the layer) to entirely cease the rotation by the magnetic braking. This time scale indicates the upper limit of the magnetic braking effect, while physical times are much smaller than τ_s (there is not any physical meaning for the resulted solutions behind this stop-time). The variations of this time scale are shown in the Figure 4 and 5 for different values of ν and density ratios $\rho(Z)/\rho_L$, respectively at the Alfvén wave speed of $1.5\,\mathrm{km s^{-1}}$ and the layer dimension of 0.2 pc. As can be seen, the stop time decreases with decreasing ν or increasing the density ratio. Also, according to the order of magnitude of non-dimensional stop times in the figures 4 and 5, and by substituting in the equation (22), the effective time scale of magnetic braking will be in the order of 10^4 years. A Gaussian function (24) was added to the density profile to investigate the existence of the condensations in the surrounding medium. The percentage difference between the integrands of the equations (28) and (17) are shown in the Figure 6. Since the percentage difference is less than 0.16%, in contrast to some studies such as Machida et al. (2011) [25], which demonstrated that the efficiency of magnetic braking on the disk formation is related to the mass of the envelope surrounding the core, our findings suggest that the existence of local Gaussian condensations in the surrounding medium does not have a significant influence on the magnetic braking of the core.

One of the astrophysical consequences of the magnetic braking phenomena is its catastrophic effect on disk disruption in the star-forming cores. Some physical mechanisms such as non-ideal MHD, turbulence, and misalignment between rotational axis and magnetic field have been proposed to weaken the magnetic braking effect. The results of this research show that the consideration of the variations of the density in the surrounding medium and/or the variations of the density ratio can change the magnetic braking time scale for one order of magnitude. Thus, regardless of the above three proposed mechanisms, increasing density slope (increasing ν) and decreasing density ratio ($\rho(Z)/\rho_L$) are somewhat effective in weakening the magnetic braking and resolving its catastrophic effect. Of course, our numerical method did not show any impressive effect of the density condensations on the issue of the magnetic braking catastrophe, and some numerical simulations should be done for more accurate calculations.

Authors' Contributions

All authors have the same contribution.

Data Availability

The data that support the findings of this study are available from the corresponding author upon reasonable request.

Conflicts of Interest

The authors declare no potential conflicts of interest.

Ethical Considerations

The authors have diligently addressed ethical concerns, such as informed consent, plagiarism, data fabrication, misconduct, falsification, double publication, redundancy, submission, and other related matters.

Funding

This research did not receive any grant from funding agencies in the public, commercial, or nonprofit sectors.

References

[1] Hennebelle, P., & Inutsuka, S.-i. 2019, Frontiers in Astronomy and Space Sciences, 6, 5.

[2] Mestel, L. 1965, QJRAS, 6, 161.

[3] Gillis, J., Mestel, L., & Paris, R. B. 1974, Ap&SS, 27, 167.

[4] Mouschovias, T. C., & Paleologou, E. V. 1980, ApJ, 237, 877.

[5] Konigl, A. 1987, ApJ, 320, 726.

[6] Basu, S., & Mouschovias, T. C. 1994, ApJ, 432, 720.

[7] Allen, A., Li, Z.-Y., Shu F. H., 2003, ApJ, 599, 363.

[8] Arfken, G. B., Weber, H. J., 2005, Mathematical Methods for Physicists. Elsevier Academic, Press, New York.

[9] Aguilar-Marin, P., Chavez-Bacilio, M., & Jauregui-Rosas, S. 2018, Eur. J. Phys., 39, 035204.

[10] Boss, A. P. 2007, ApJ, 685, 1136.

[11] Boss, A. P. 2009, ApJ, 97, 1940.

[12] Codella, C., Cabrit, S., Gueth, F., Podio, L., Leurini, S., Bachiller, R., Gusdorf, A., Lefloch, B., & Nisini, B. 2014, A&A, 568, L5.

[13] Dapp, W. B., & Basu, S. 2010, A&A, .521, 4.

[14] Dapp, W. B., Basu, S., & Kunz, M. W. 2012, A&A, .541, 18.

[15] Fehér, O., Tóth, L. V., Ward-Thompson, D., Kirk, J., Kraus, A., Pelkonen, V. M., Pintér, S., & Zahorecz, S. 2016, A&A, 590, A75.

[16] Galli, D., Lizano, S., Shu, F. H., & Allen, A. 2006, ApJ, 647, 374.

[17] Galli, D., Cai, M., Lizano, S., & Shu, F. H. 2009, RMxAC, 36, 143.

[18] Joos, M., Hennebelle, P., & Ciardi, A. 2012, A&A, 543, 22.

[19] Koley, A. 2022, MNRAS,516, 185.

[20] Krumholz, M. R., Crutcher, R. M., & Hull, C. L. H. 2013, ApJL, 767, L11.

[21] Langer, W. D., Velusamy, T., Kuiper, T. B. H., Levin, S., Olsen, E., & Migenes, V. 1995, ApJ, 453, 293.

[22] Lee, C.-F., Li, Z.-Y., Ho, P. T. P., Hirano, N., Zhang, Q., & Shang, H. 2017, Sci. Adv., 3, e1602935.

[23] Li, Z.-Y., Krasnopolsky, R., & Shang, H. 2013, ApJ, 774, 12.

[24] Lam, K. H., Li, Z. -Y., Chen, C. -Y., Tomida, K., & Zhao, B. 2019, MNRAS, 482, 5326.

[25] Machida, M. N., Inutsuka, S.-I., & Matsumoto, T. 2011, PASJ, 63, 555.

[26] Marchand, P., Commerçon, B., & Chabrier, G. 2018, A&A, 619, 16.

[27] Mellon, R. R., & Li, Z.-Y. 2008, ApJ, 681, 1356.

[28] Mellon, R. R., & Li, Z.-Y. 2009, ApJ, 698, 922.

[29] Molina-Bolivar, J. A., & Abella-Palacios, A. J. 2012, Eur. J. Phys, 33, 697.

[30] Nakano, T. 1989, MNRAS, 241, 495 (N89).

[31] Pasquale, O., & Ambrosis, A. D., 2012, Am. J. Phys., 80, 27.

[32] Press, W. H., Teukolsky, S. A., Vetterling, W. T., & Flannery, B. P. 1992, Numerical recipes in FORTRAN 77: The art of scientific computing. Cambridge University Press, New York.

[33] Santos-Lima, R., de Gouveia Dal Pino, E. M., & Lazarian, A. 2012, ApJ, 747, 21.

[34] Seifried, D., Banerjee, R., Pudritz, R. E., & Klessen, R. S. 2012, MNRAS, 423, L40.

[35] Seifried, D., Banerjee, R., Pudritz, R. E., & Klessen, R. S. 2013, MNRAS, 432, 3320.

[36] Stahler, S. W., & Palla, F. 2004, The Formation of Stars. Wiley-VCH, New York.

[37] Tomida, K., Okuzumi, S., & Machida, M. N. 2015, MNRAS, 801, 20.

[38] Tsukamoto, Y., Iwasaki, K., Okuzumi, S., Machida, M. N., & Inutsuka S. 2015a, MNRAS, 452, 278.

[39] Tsukamoto, Y., Iwasaki, K., Okuzumi, S., Machida, M. N., & Inutsuka S. 2015b, ApJL, 810, L26.

[40] Unofre, B. P. 2020, Phys. Educ., 55, 035025.

[41] Vaytet, N., Commerçon, B., Masson J., González, M., & Chabrier, G. 2018, A&A, 615, 18.

[42] Wurster, J., Bate, M. R., & Price, D. J. 2016, MNRAS, 547, 1037.

[43] Wurster, J., Bate, M. R., & Price, D. J. 2019, MNRAS, 489, 1719.

[44] Wurster, J. 2021, MNRAS, 501, 5873.

[45] Yen, H.-W., Koch, P. M., Hul, C. L. H., Ward-Thompson, D., Bastien, P., Hasegawa, T., Kwon, W., Lai, S.-P., Qiu, K., & Ching, T.-C. 2021, ApJ, 907, 33.

[46] Zhao, B., Caselli, P., Li, Z. -Y., Krasnopolsky, R., Shang, H., & Nakamura, F. 2016, MNRAS, 460, 2050.

[47] Zhao, B., Caselli, P., Li, Z. -Y., Krasnopolsky, R. 2018, MNRAS, 473, 4868.

[48] Zhao, B., Caselli, P., Li Z. -Y., Krasnopolsky, R., Shang, H., & Lam, K. H. 2021, MNRAS, 505, 5142.